C.P. No. 583

C.P. No. 583

MINISTRY OF AVIATION

AERONAUTICAL RESEARCH COUNCIL

CURRENT PAPERS

Surface Oil-Flow Patterns on Wings of Different Leading-Edge Radius and Sweepback

H. C. Garner, M.A., A.F.R.Ae.S.,
and
Miss D. K. Cox, B.Sc.,

of the Aerodynamics Division,
National Physical Laboratory

LONDON: HER MAJESTY'S STATIONERY OFFICE

1962

PRICE 5s 6d NET

C.P. No.583

Surface Oil-Flow Patterns on Wings of Different Leading-Edge Radius and Sweepback

- By -
H. C. Garner, M.A., A.F.R.Ae.S.,
and
Miss D. K. Cox, B.Sc.
of the Aerodynamics Division,
National Physical Laboratory

March, 1961

Summary

The influence of leading-edge radius and sweepback on the development of leading-edge vortices has been studied by means of surface oil-flow patterns. The model was designed to have four different angles (45°, 49.4°, 55° and 60°) of leading-edge sweepback and four profiles normal to the leading edge of widely varying nose radius.

A qualitative discussion of the oil-flow patterns considers in turn the effects of Reynolds number, incidence, sweepback and profile, with particular reference to the phenomenon of leading-edge flow reversal. It appears that nose shape has little influence on the incidence at which leading-edge flow reversal occurs.

There follows a numerical analysis of the incidences at which a leading-edge vortex forms, especially the range of incidence during which the origin of the vortex traverses the leading edge from tip to leading apex; an approximate formula for this range is discussed. The data on leading-edge flow reversal suggest a rough linear relationship between incidence and a critical angle of leading-edge sweepback below which leading-edge flow reversal is apparent.

The Appendix describes a new and successful procedure for the photo-reproduction of surface oil-flow patterns.

Contents

References/

Previously issued as NPL/Aero/415 - A.R.C.22,814.
Published with the permission of the Director, National Physical Laboratory.

---

1. Introduction

The development of leading-edge vortices from swept wings at incidence undergoes a decisive change in the range of leading-edge sweepback from 45° to 60°. At 45°, the vortex first appears at moderately high incidence and diffuses rapidly by the mechanism of vortex breakdown, while at 60° the vortex appears at a relatively low incidence and can persist as a compact vortex for a distance comparable with the dimensions of the planform. The influence of leading-edge radius on the formation of these vortices has been studied by means of surface oil-flow patterns on a model having variable sweepback and four interchangeable front portions of differing nose shape.

The oil-flow technique for visualization of surface flow in low-speed tunnels has been in use for a considerable number of years[1,2]. The technique consists of coating a model with a thin film of oil mixture containing a suspension of titanium dioxide and then observing the pattern that develops on the surface as the oil evaporates during a tunnel run. Details of the technique are fully discussed in Ref. 2. A theoretical solution for the motion of the oil film is given in Ref. 3; it is deduced that the oil flows in the direction of the boundary-layer skin friction, except near separation, where the oil tends to indicate separation too early. Moreover, the oil flow scarcely disturbs the motion of the air within the boundary layer. It is important, nevertheless, to avoid a surfeit of oil near the leading edge where the boundary layer is very thin.

Maskell[4] has considered in general terms the concept of three-dimensional flow separation and the characteristic patterns formed on a wing surface by the limiting streamlines. These will start at the leading edge or from some other attachment line and will end at the trailing edge or at some other separation line. An attachment line is thus the boundary between diverging surface flows, while two surface flows converge on either side of a separation line. When both converging flows are discernible from the oil patterns, the separation line is well defined. Often, however, there is a region of low shear on one side of the separation line and no indication of limiting streamlines. Then, according to Ref. 3, the oil pattern on the opposite side may indicate separation rather too early, but still gives a reliable qualitative picture of the local flow.

2. Description of Model and Tests

The investigation covered four angles of leading-edge sweepback (Λ_L = 45°, 49.4°, 55°, 60°) and four aerofoil sections. The variation in planform was effected by a combination of two rotatable half-wings and complementary portions to fill the central gaps fore and aft. The basic planform (Λ_L = 49.4°) with streamwise tips was that of the cropped arrowhead wing in Ref. 5. All four planforms are illustrated in Fig. 1, and their root chord c_r, geometric mean chord $\bar{c}$, semi-span s and aspect ratio $A = 2s/\bar{c}$ are given in the following table.

Table/

Λ_L	c_r (in.)	$\bar{c}$ (in.)	s (in.)	A
45°	17.96	12.31	18.71	3.040
49.4°	19.20	13.33	17.60	2.640
55°	21.33	14.44	16.82	2.330
60°	24.00	15.83	16.03	2.026

The basic aerofoil section was also that of Ref. 5; that is to say, in the case $\Lambda_L = 49.4°$ the streamwise section was that of a 10 per-cent-thick RAE 102 aerofoil[6]. The maximum thickness occurs at 0.356 chord, and alternative portions forward of this were designed to have leading-edge radii 0.01756c, 0.00686c, 0.00268c and 0.00110c, the second of which corresponds to the basic aerofoil. More relevant to the present problem and independent of the angle of sweepback is the profile at right angles to the leading edge, and the respective profiles A, B, C and D are shown in Fig. 2. The calculated leading-edge radii in planes normal to the leading edge vary linearly from tip to root.

Profile	Normal to leading edge	
	$(\rho_L)_{tip}$	$(\rho_L)_{root}$
A	0.201 in.	0.518 in.
B	0.079 in.	0.202 in.
C	0.031 in.	0.079 in.
D	0.013 in.	0.032 in.

The size of the forward central portion will slightly affect $(\rho_L)_{root}$, and the tabulated values correspond to $\Lambda_L = 49.4°$. Unfortunately, it was discovered after the tests that profile B was incorrectly contoured near the leading edge, so that the oil-flow patterns are not directly comparable with those in Ref. 5. Profile B, as shown in Fig. 2, is based on the actual model whose leading edge was rather too blunt.

Oil-flow patterns were photographed with a camera mounted beneath the floor of the South 9 ft by 7 ft Wind Tunnel. To minimise distortion error, the photographic plate was arranged parallel to the plane of the wing at a fixed incidence to which the wing was set after the patterns had developed; nevertheless the planforms sometimes appear to be distorted. Tangential flash lighting was used to obtain the best contrast.

Table 1/

Table 1 lists 29 oil-flow patterns and the figures where they appear. Other oil patterns, photographed but not reproduced, are used in the analysis. The incidence α is nominal and uncorrected. The Reynolds numbers $R = V\bar{c}/\nu$ correspond to $V = 90$ and 150 ft/sec, to an average value of $\bar{c}$ (ft) and $\nu = 1.56 \times 10^{-4}$ ft^2/sec; as usual the quality of the patterns is less good at the lower speed. For $\Lambda_L = 49.4°$, 55° and 60° the joins between the central forward portion and the rest of the wing are apparent, and so are those at the edge of the central rear portion for $\Lambda_L = 45°$, 49.4° and 55°; in all cases the joins between the main forward and rear portions of the wing are clearly seen. Although these various joins break the continuity of the flow lines, they neither cause discontinuity in flow direction nor hamper the interpretation of the oil patterns.

3. Discussion of Oil-Flow Patterns

Figs. 3a to 3d illustrate the effect of leading-edge sweepback for the two Reynolds numbers and profiles B, C and D. Figs. 4a and 4b show the effect of incidence for $\Lambda_L = 49.4°$ and 55° respectively. Figs. 5a and 5b show the effect of profile for $\Lambda_L = 49.4°$ and 60° respectively. The effect of Reynolds number is illustrated further in Fig. 6. These will now be discussed qualitatively by considering in turn the non-dimensional parameters Reynolds number, incidence, sweepback and profile (Fig. 2).

3.1 Effect of Reynolds number

As found in Refs. 5 and 7, an increase in Reynolds number tends to delay the incidence at which a leading-edge vortex first forms. This effect is probably associated with the more rapid development of attached turbulent flow following an initial laminar separation. There is some evidence from preliminary tests in the Compressed Air Tunnel on the model of profile C and $\Lambda_L = 60°$, that the effect persists at Reynolds numbers $R = 10^7$ and above. Once a full-span leading-edge vortex is established, changes in Reynolds number become less important.

Apart from the better quality of oil patterns at the higher speed, Fig. 6 and the comparisons of Figs. 3a and 3b show no major effect of Reynolds number. There is, however, a general tendency for the secondary separation line to be closer to the leading edge at the higher Reynolds number; this is especially true at the highest sweepback.

3.2 Effects of incidence

As incidence increases, the leading-edge vortex first forms near the tip and then the origin of the vortex traverses the leading edge until it reaches the apex of the wing. There is thus a range of incidence during which a part-span vortex is present; for a given wing this range will depend on Reynolds number. Practically all the illustrated oil patterns show full-span leading-edge vortices and correspond to incidences outside the range. An analysis of patterns at lower incidences in Section 4 suggests a simple manner in which the range may depend on sweepback and nose radius.

Above a certain incidence, vortex breakdown will occur in the neighbourhood of the wing. It is often found that at a somewhat higher incidence the secondary separation line appears to stop short of the wing tip, so that the surface flow turns inboard; this is termed leading-edge flow reversal. Figs. 4a and 4b illustrate how this effect spreads towards the apex as incidence increases for profiles B and C and $\Lambda_L = 49.4°$ and 55°. The incidence at which leading-edge flow reversal becomes prominent is seen to increase with sweepback, but not to depend much on aerofoil profile.

3.3/

3.3 Effects of sweepback

The effects of sweepback are best illustrated in Fig. 3b. This shows how for profile B and a fixed incidence $\alpha = 16°$ the oil patterns change systematically as Λ_L increases from 45° to 60°. At $\Lambda_L = 45°$ the origin of the vortex is at an appreciable distance from the leading apex, and leading-edge flow reversal occurs very close to this origin. It would thus appear that vortex breakdown is almost coincident with vortex formation. The absence of an attachment line inboard of the "eye" suggests that a large proportion of the upper-surface boundary layer is induced to flow under a diffuse vortex. It is now established that appreciable changes in surface pressure occur downstream of a vortex breakdown[8] (Lambourne and Bryer, 1961); the allied pressure field may well induce a low-energy forward flow close and parallel to the leading edge.

A small increase in sweepback to $\Lambda_L = 49.4°$ causes the origin to move to the apex. The "herring-bone" attachment line and secondary separation line are clearly seen over the inner part of the wing, whilst the flow near the outer half of the leading edge is hardly changed. A further increase to $\Lambda_L = 55°$ displaces the leading-edge flow reversal to a position fairly close to the tip; the typical inboard and outboard flows are maintained. Finally at $\Lambda_L = 60°$ the oil pattern shows no trace of the flow reversal.

Fig. 3c gives the corresponding sequence for profile C at the same incidence and Reynolds number. With the sharper leading edge there is a tendency for the secondary separation line and the "eye" to be further from the leading edge; nevertheless the smaller nose radius scarcely influences the spanwise location of leading-edge flow reversal. With the smallest radius of all, the full-span vortex is established at a much lower incidence (Fig. 3d); the flow reversal then affects only a small region, and over much of the span the type of flow is essentially independent of sweepback in the range $45° \leqslant \Lambda_L \leqslant 60°$. A quantitative analysis of the critical leading-edge sweepback for leading-edge flow reversal is attempted in Section 5.

3.4 Effects of profile

We have seen from Figs. 3b to 3d that leading-edge radius has a fairly small effect on the location of flow reversal. An exception to this is the roundest profile A. Fig. 5a includes a distinctive oil pattern for $\Lambda_L = 49.4°$ and $\alpha = 20°$, which might be explained in terms of a particularly violent vortex breakdown. With such a large leading-edge radius the initial formation of a part-span vortex at some spanwise position will be delayed until an incidence greater than that for which breakdown and flow reversal would otherwise have occurred close to the origin.

The corresponding oil pattern for profile A at $\Lambda_L = 60°$ in Fig.5b has traces of features observed on the 9% thick curved-tip wing of the same sweepback in Ref. 7. That is to say, the main vortex has no clear origin and first appears at a considerable distance from the leading edge; moreover, there is the significant "dead-air region" extending between the initial and secondary separation lines and also the additional leading-edge vortex further outboard. The "eye" outboard of the latter vortex indicates that the flow reversal is just becoming significant.

The primary effect of decreasing leading-edge radius is to intensify the adverse pressure gradients near the leading edge, so as to cause vortex formation at a lower incidence. Figs. 5a and 5b show vortices at similar stages of development for the four profiles with $\Lambda_L = 49.4°$ and 60° respectively. The incidence ranges from $\alpha = 20°$ for profile A to $\alpha = 10°$

for/

for profile D. A further deduction is that, the higher the sweepback, the less important are the effects of profile on the type of flow. Thus, when $\Lambda_L = 49.4°$ we contrast the oil patterns for profiles A and B with those for profiles C and D, while only profile A is distinctive when $\Lambda_L = 60°$. It must be stressed, however, that the profiles of Fig. 2 are normal to the leading edge and independent of sweepback. In practice, a wing of very high sweepback would be designed with a relatively thick normal profile; as in Ref. 7, a change of profile may then be of fundamental importance.

4. Numerical Analysis

One purpose of the present investigation is to discover the non-dimensional parameters that control the formation of a leading-edge vortex. It has already been mentioned that increases in Reynolds number and leading-edge radius discourage the vortex, while increases in incidence and leading-edge sweepback encourage it. It is to be expected that the local peak suction coefficient near the leading edge will play an important role. This cannot readily be estimated on a three-dimensional wing with any precision, but consideration of two-dimensional flow past a symmetrical aerofoil leads to the simple approximate result

$$(-C_p)_{max} = \left(\frac{2c}{\rho_L} - 1\right) \sin^2 \alpha \, . \qquad \ldots (1)$$

This follows from Ref. 9 or Ref. 10, provided that the aerofoil thickness and ρ_L are not too large and α is not too small.

Equation (1) suggests that the parameter $\alpha^2 c/\rho_L$ may be helpful in attempting a rough correlation between local leading-edge radius and the incidence at which a part-span vortex forms there. An analysis of oil-flow patterns at moderately small incidences shows that within about ±20% the condition for the existence of a leading-edge vortex is that

$$\alpha \text{ (deg)} > \sqrt{k\rho_L \cos \Lambda_L} \, , \qquad \ldots (2)$$

where for these experiments $k = 2000$ (inches)$^{-1}$ and ρ_L is the local nose radius of the profile normal to the leading edge in inches. It would follow from (2) that the range of incidence for part-span vortices in the present experiments is

$$\sqrt{2000\,(\rho_L)_{tip} \cos \Lambda_L} \leqslant \alpha \leqslant \sqrt{2000\,(\rho_L)_{root} \cos \Lambda_L} \, , \qquad \ldots (3)$$

where $(\rho_L)_{tip}$ and $(\rho_L)_{root}$ are tabulated in Section 2.

The results for profiles B, C and D are presented in Fig. 7, where the bounds of equation (3) are compared with the range of incidence estimated from the available oil patterns. The lower bound for leading-edge vortex flow is represented fairly well by the approximate formula. The upper bound is of less consequence; the higher incidences from experiment might be expected, since the leading apex causes the peak suction coefficient to fall in the neighbourhood of the root. This effect is too localized to be very important, but the centre section can be treated on the basis of Section 5 of Ref. 10. The lower bound of equation (3) overestimates the incidence at which a part-span vortex occurs with profile A; however, this may be attributed to the distinctive types of flow that are discussed in Section 3.4.

It/

It is not yet clear how the quantities k and ρ_L in equation (2) should be non-dimensionalized to take account of Reynolds number, though forthcoming experiments in the Compressed Air Tunnel may settle the question. It may then be possible to consider the applicability of a generalized parametric condition for the formation of a leading-edge vortex.

5. Critical Sweepback for Leading-Edge Flow Reversal

It may be helpful to consider a given normal profile and a given incidence, and to enquire from the oil patterns at what leading-edge sweepback the secondary flow reversal (Section 3.2) appears; as critical cases we take the following,

Profile	Λ_L	α	Oil-flow pattern
B	55°	16°	Fig. 3b bottom left
D	49.4°	10°	Fig. 3d top right
A	60°	20°	Fig. 5b top left

which all show a small but significant tip region of the leading edge with reverse flow. These and other interpolated data are plotted in Fig. 8. A rough conclusion is that there is a linear relationship between $(\Lambda_L)_{crit}$ and α, such that leading-edge flow reversal is only present if $\Lambda_L < (\Lambda_L)_{crit}$; the condition is apparently independent of nose shape.

6. Acknowledgements

The authors wish to acknowledge the help of the Central Photographic Section, N.P.L., and of Miss B. A. Foster who assisted with the experimental work. The authors are indebted to Mr. E. C. Maskell of the Royal Aircraft Establishment for pointing out the difficulty of locating vortex breakdown from oil-flow patterns; they also acknowledge helpful discussions on this question with Mr. N. C. Lambourne and Mr. D. W. Bryer of the Aerodynamics Division, N.P.L.

References/

References

No.	Author(s)	Title, etc.
1	J. Black	A note on the vortex pattern in the boundary layer of a sweptback wing. Jour. Roy. Aero. Soc., Vol.56, p.279. 1952.
2	R. L. Maltby and R. F. A. Keating	Flow visualization in low-speed wind tunnels: current British practice. A.R.C.22,373. August, 1960.
3	L. C. Squire	The motion of a thin oil sheet under the boundary layer on a body. A.R.C.21,988. February, 1960.
4	E. C. Maskell	Flow separation in three dimensions. A.R.C.18,063. November, 1955.
5	H. C. Garner and D. W. Bryer	Experimental study of surface flow and part-span vortex layers on a cropped arrowhead wing. A.R.C. R. & M.3107. April, 1957.
6	R. C. Pankhurst and H. B. Squire	Calculated pressure distributions for the RAE 100-104 aerofoil sections. A.R.C. C.P.80. March, 1950.
7	H. C. Garner and D. E. Walshe	Pressure distribution and surface flow on 5% and 9% thick wings with curved tip and 60° sweepback. A.R.C. R. & M.3244. January, 1960.
8	N. C. Lambourne and D. W. Bryer	The bursting of leading-edge vortices. Some observations and discussion of the phenomenon. A.R.C.22,775. April, 1961.
9	S. Goldstein	Approximate two-dimensional aerofoil theory. Part I. Velocity distributions for symmetrical aerofoils. A.R.C. C.P.68. May, 1942.
10	J. Weber	The calculations of the pressure distribution over the surface of two-dimensional and swept wings with symmetrical aerofoil sections. A.R.C. R. & M.2918. July, 1953.

APPENDIX/

APPENDIX

An Improved Procedure for the
Photo-Reproduction of Oil-Flow Patterns
- By -
C. C. Fane
of Central Photographic Section

The normal procedure for producing a set of Photostat prints from photographs of surface oil-flow patterns is as follows:

A1. A negative is produced by normal photography.

A2. A special "soft" print is made from the negative by enlargement.

A3. A Photostat negative is made from the soft print.

A4. The final Photostat positive is produced from the negative.

All of these stages involve the use of a lens, namely, a camera lens in A1, an enlarging lens in A2, and a Photostat camera lens in A3 and A4. The definition of the final print also suffers because only half of the precedure is under the control of a skilled photographer, while the rest involves the limitations of the Photostat process.

It was decided that improved definition of the final print could be achieved by the following procedure:

B1. A negative is produced by normal photography.

B2. A contact positive transparency from the negative is produced on an E.M.I. electronic printer which incorporates automatic shading.

B3. A negative print is produced from the transparency by normal enlarging methods.

B4. A final Photostat positive is made directly from the negative print.

There is now no lens systems in the second stage, and only a quarter of the procedure involves the Photostat process. Between stages B3 and B4 the negative print is mounted on matt black paper and the captions are stencilled in Process White ink.

A light, fairly soft print was found to be ideal in stage B3. Only then was it possible to differentiate between the darker areas of the negative print and the black background. Moreover, this served to reduce the exposure at the Photostat camera and preserve a white background to the final print.

In the normal procedure an amount of shading had to be done at stage A2 in order to bring the overall contrast down to a workable Photostat level. This was out out almost entirely by the use of the E.M.I. electronic printer.

Table 1/

Table 1

Summary of Oil-Flow Patterns

Λ_L	Profile	α	R x 10^{-6}	Fig(s).
45	B	16	0.7	3a
45	B	16	1.1	3b
45	C	16	1.1	3c
45	D	10	1.1	3d
49.4	A	20	1.1	5a
49.4	B	12	1.1	4a
49.4	B	16	0.7	3a
49.4	B	16	1.1	3b,5a
49.4	B	20	1.1	4a
49.4	C	12	1.1	4a,5a
49.4	C	16	1.1	3c
49.4	C	20	1.1	4a
49.4	D	10	1.1	3d,5a
55	B	13	1.1	4b
55	B	16	0.7	3a
55	B	16	1.1	3b
55	B	22	1.1	4b
55	C	10	1.1	4b
55	C	16	1.1	3c,4b
55	D	10	1.1	3d
60	A	16	0.7	6
60	A	16	1.1	6
60	A	20	1.1	5b
60	B	16	0.7	3a
60	B	16	1.1	3b,5b
60	C	12	0.7	6
60	C	12	1.1	5b,6
60	C	16	1.1	3c
60	D	10	1.1	3d,5b

N.P.L./AERO/415

FIG. 1

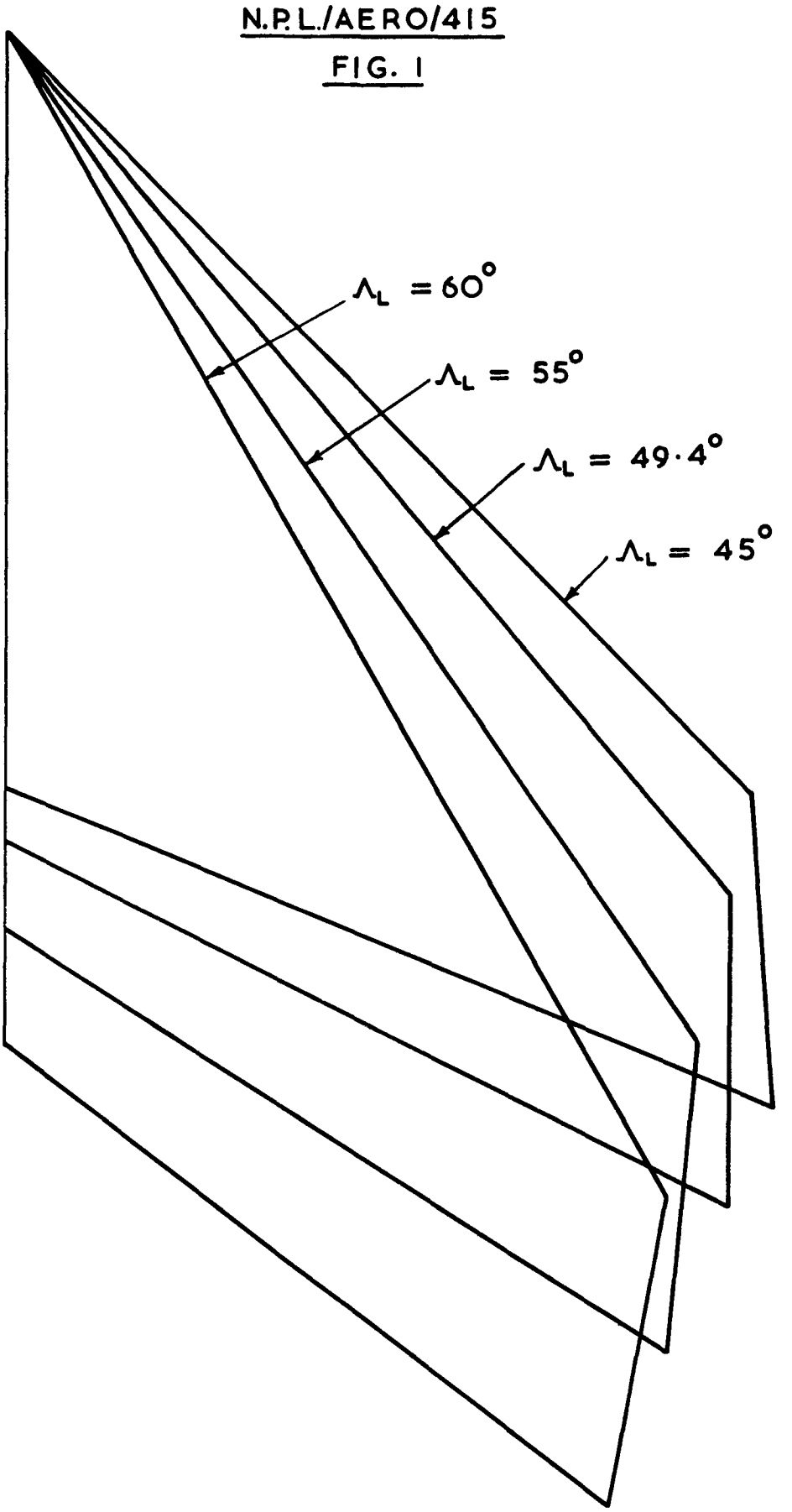

Four half-planforms of different leading-edge sweepback

j. a. p.

N.P.L./AERO/415

FIG. 2

Profile A

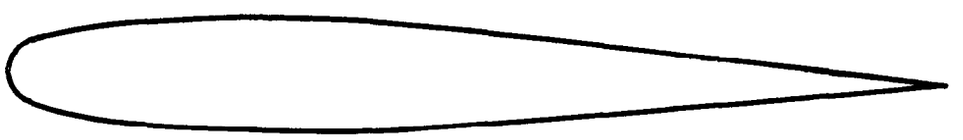

Profile B

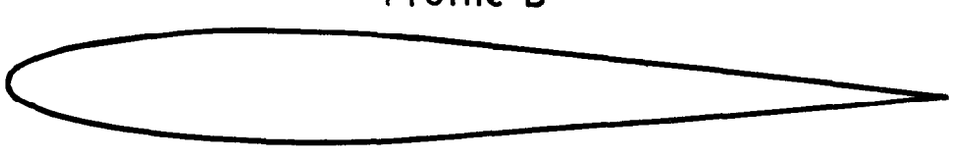

Profile C

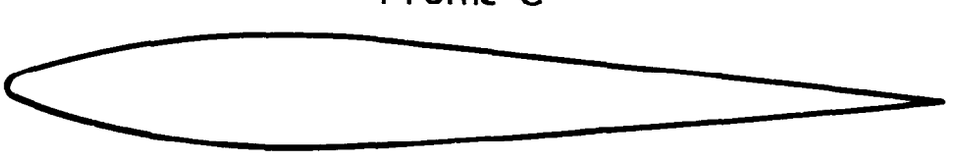

Profile D

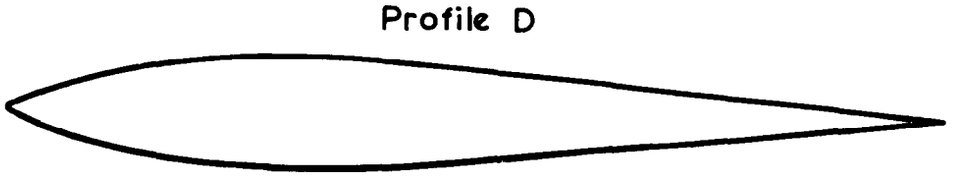

Four profiles normal to the leading edge of different nose radius

j.a.p.

FIG. 3a

PROFILE B $\alpha = 16^\circ$ $R = 0{\cdot}7 \times 10^6$

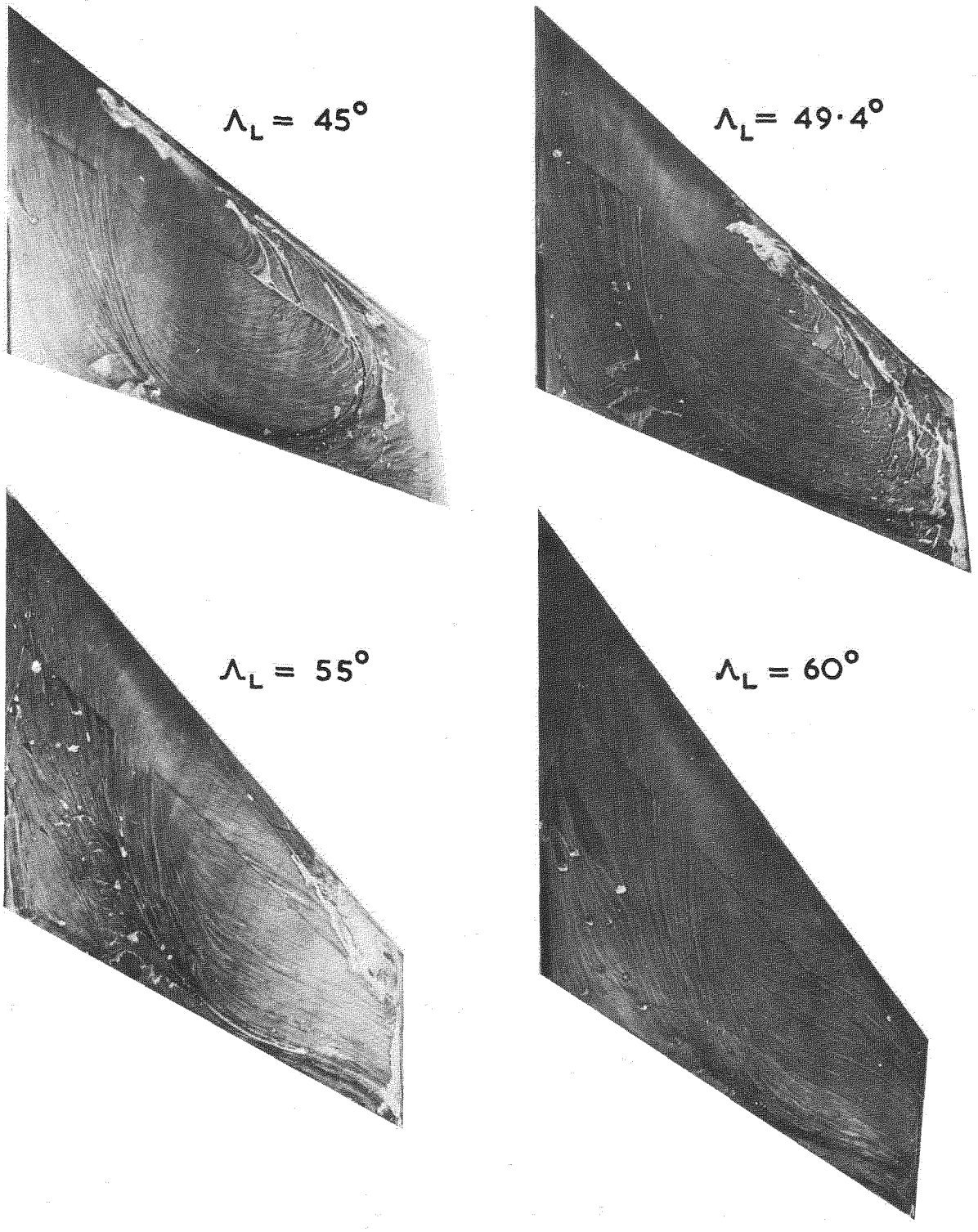

OIL PATTERNS SHOWING THE EFFECT OF SWEEPBACK

FIG. 3 b

PROFILE B $\alpha = 16^\circ$ $R = 1{\cdot}1 \times 10^6$

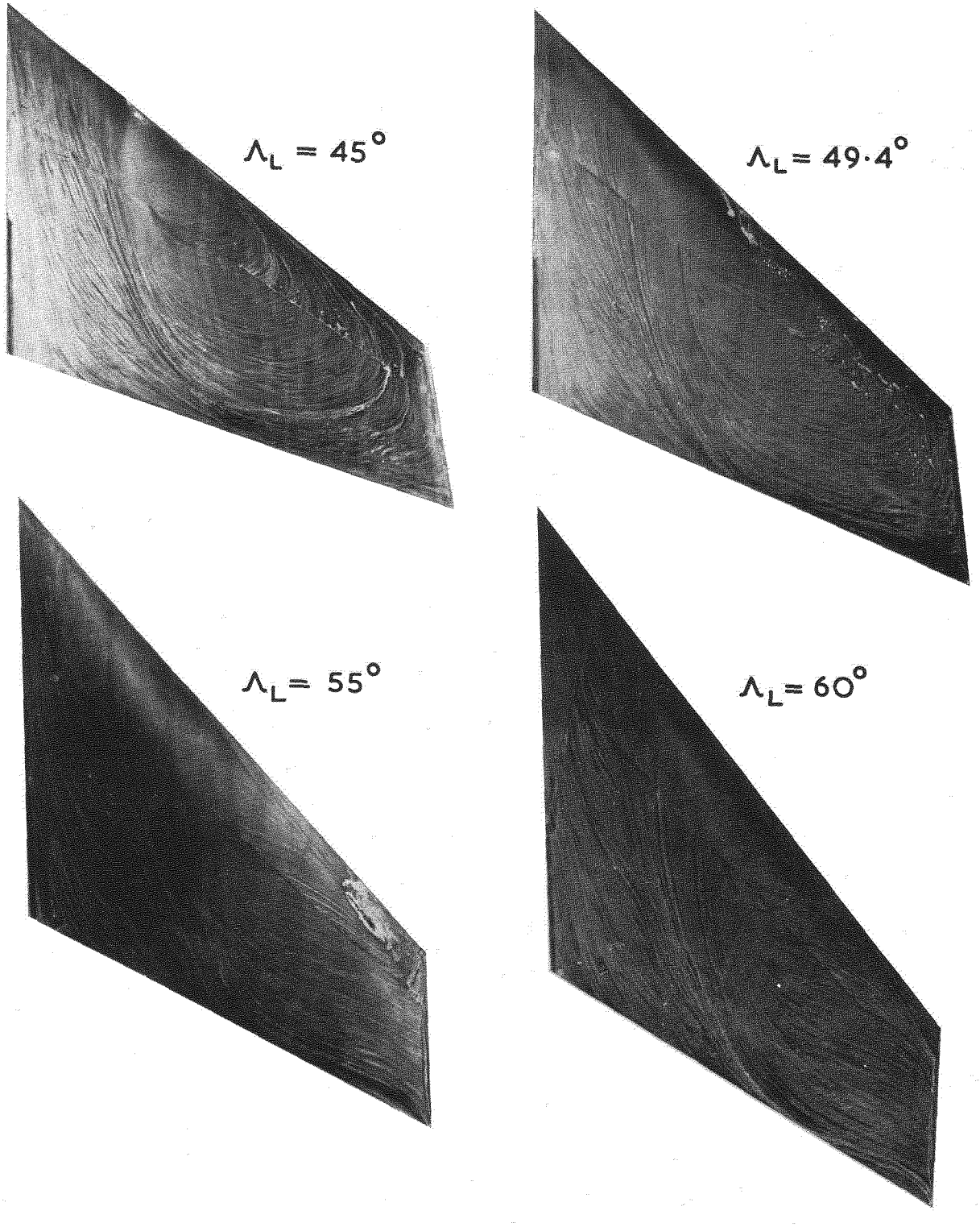

OIL PATTERNS SHOWING THE EFFECT OF SWEEPBACK

FIG.3c

PROFILE C $\alpha = 16^\circ$ $R = 1{\cdot}1 \times 10^6$

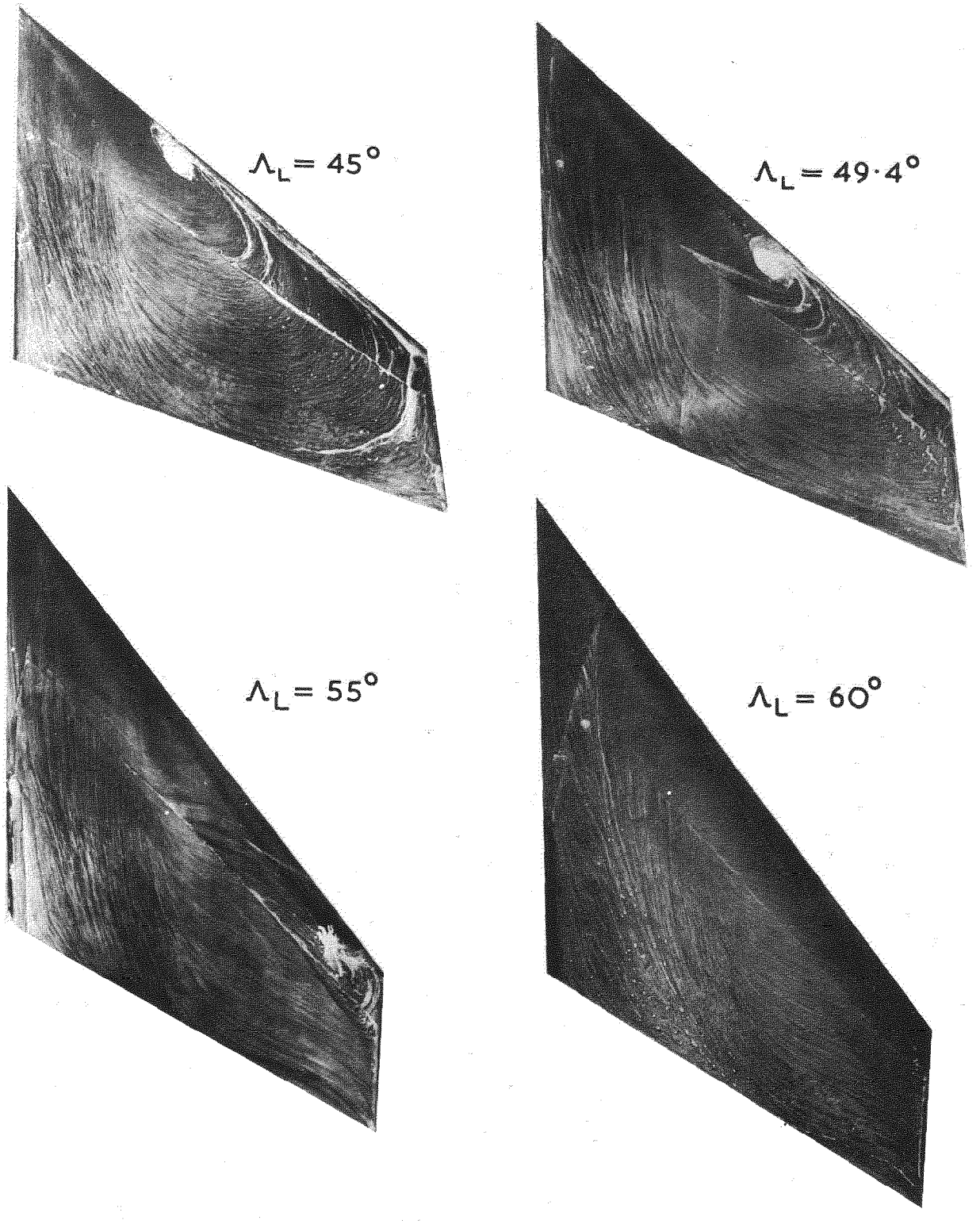

OIL PATTERNS SHOWING THE EFFECT OF SWEEPBACK

FIG. 3d

PROFILE D $\alpha = 10^\circ$ $R = 1{\cdot}1 \times 10^6$

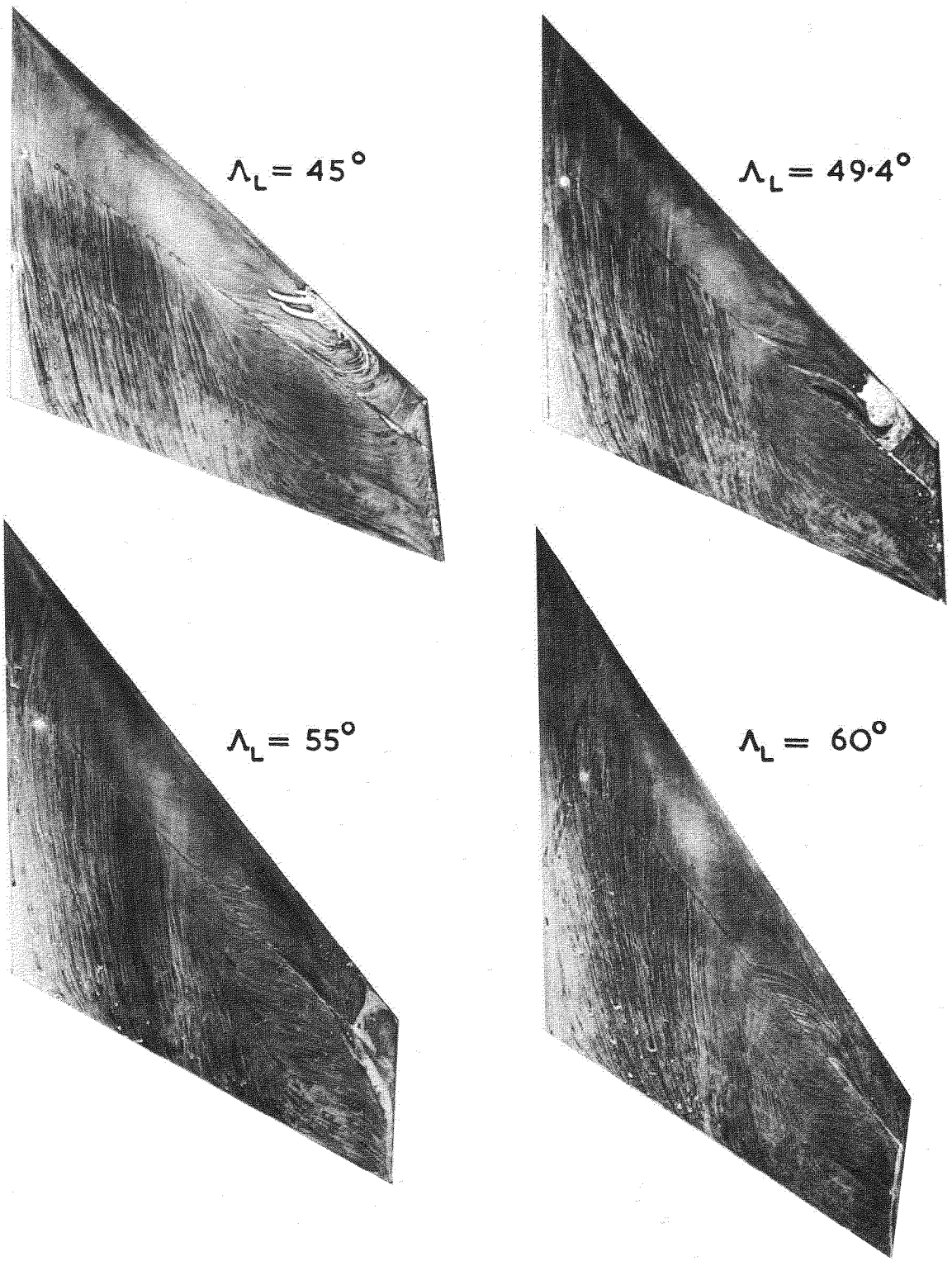

OIL PATTERNS SHOWING THE EFFECT OF SWEEPBACK

FIG. 4a

$\Lambda_L = 49{\cdot}4°$ $R = 1{\cdot}1 \times 10^6$

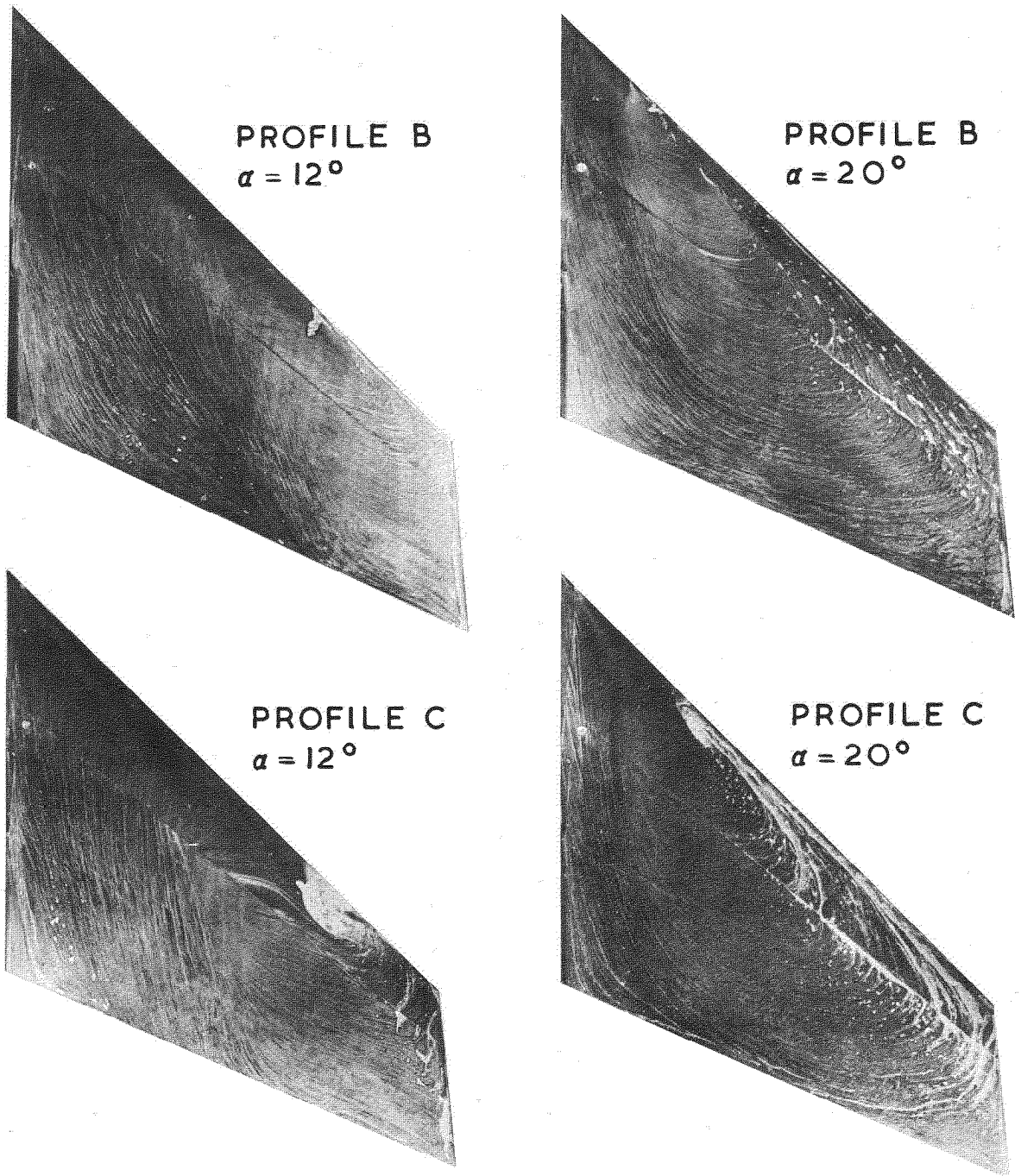

OIL PATTERNS SHOWING THE EFFECT OF INCIDENCE

FIG. 4 b

$\Lambda_L = 55^\circ$ $R = 1{\cdot}1 \times 10^6$

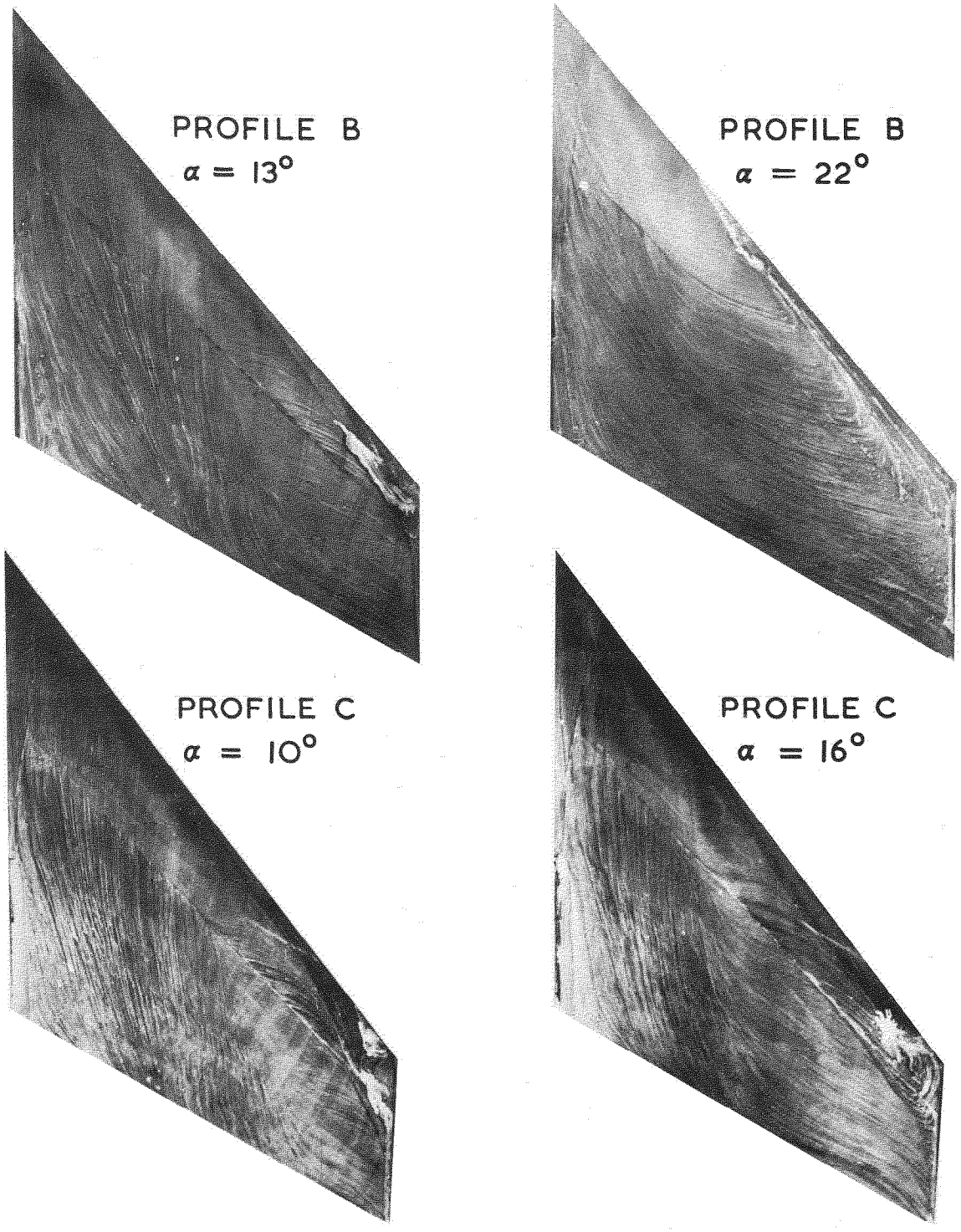

OIL PATTERNS SHOWING THE EFFECT OF INCIDENCE

FIG. 5a

$\Lambda_L = 49{\cdot}4°$ $R = 1{\cdot}1 \times 10^6$

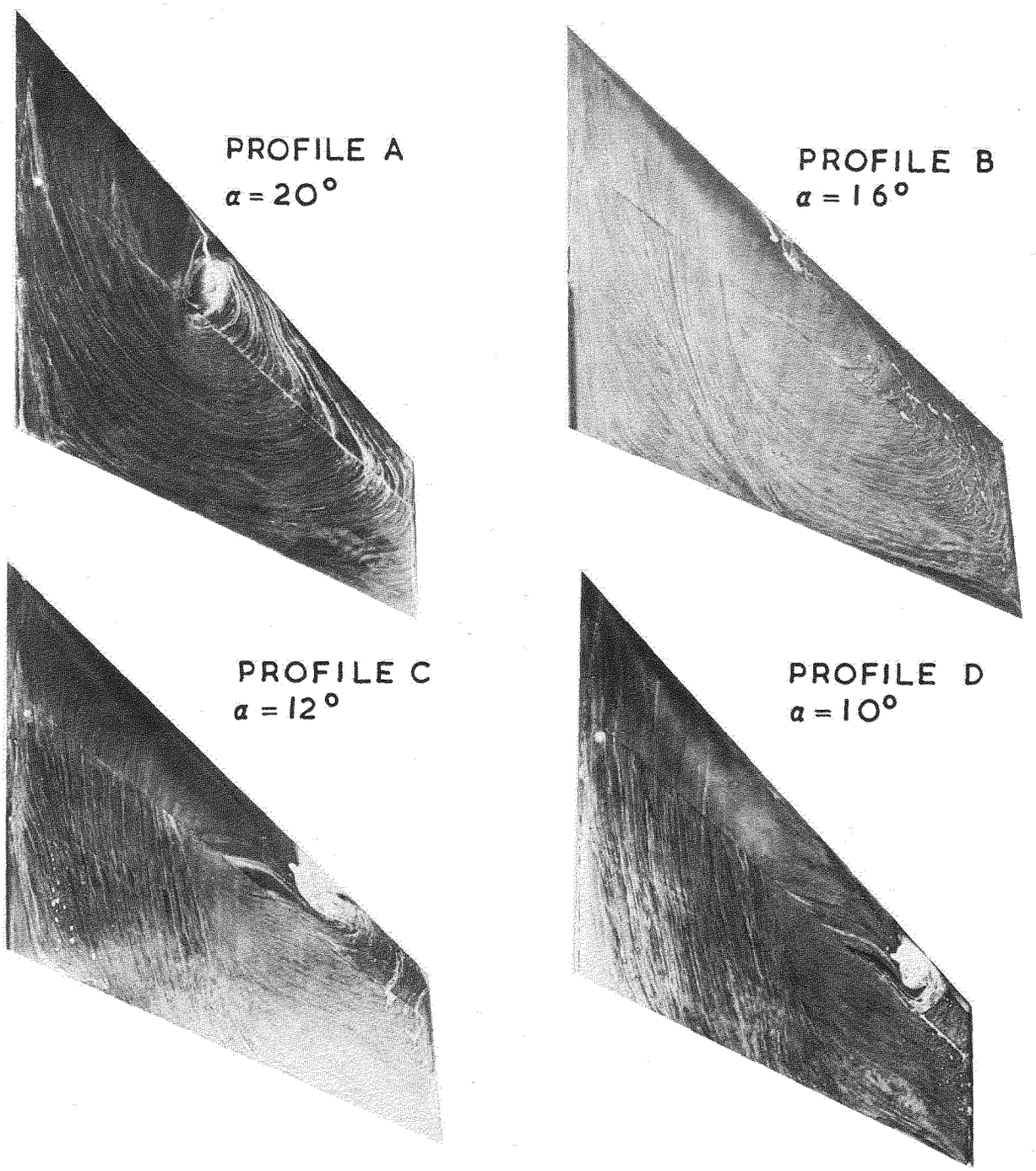

OIL PATTERNS SHOWING THE EFFECT OF PROFILE

FIG. 5b

$\Lambda_L = 60°$ $R = 1{\cdot}1 \times 10^6$

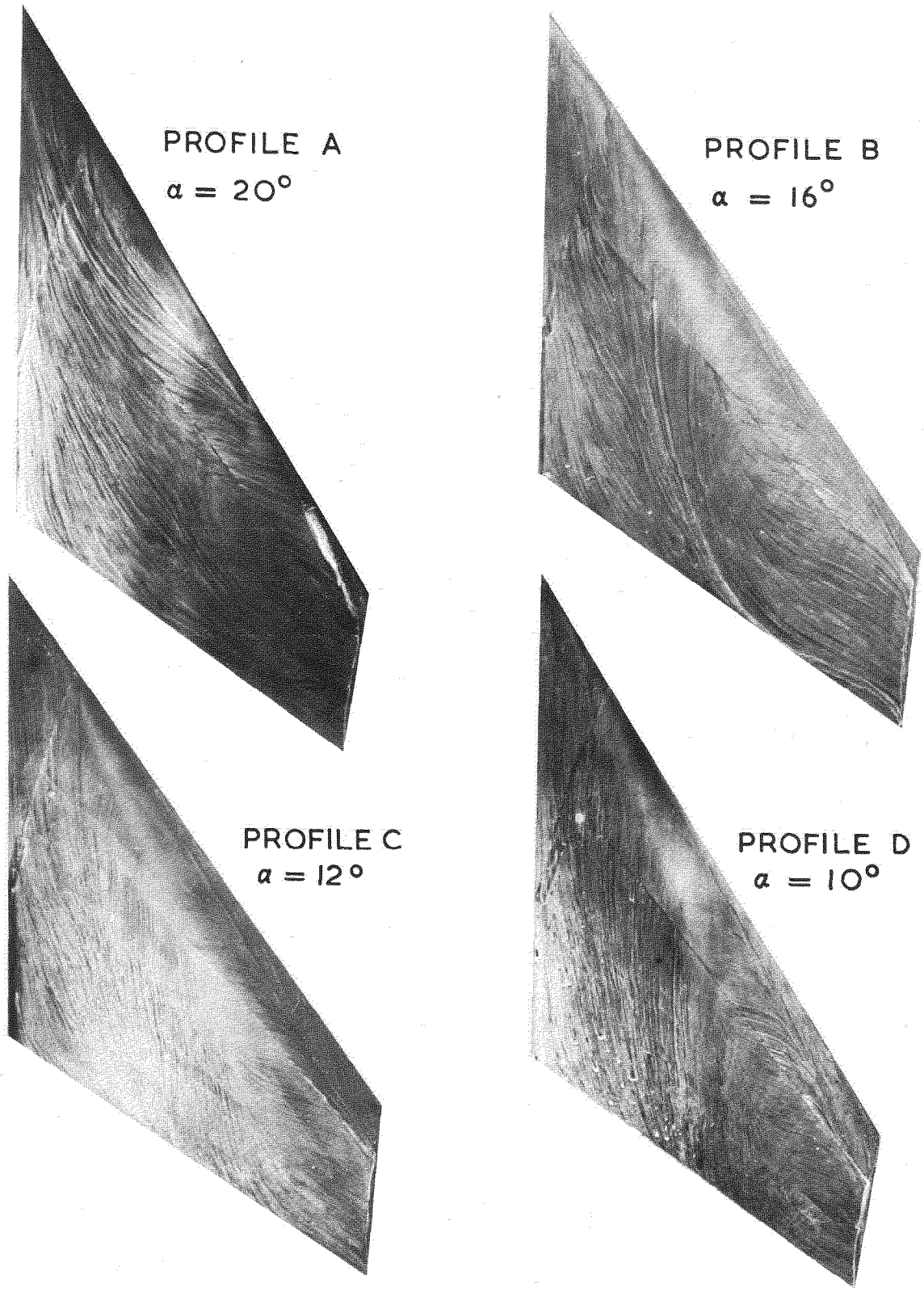

OIL PATTERNS SHOWING THE EFFECT OF PROFILE

FIG. 6

$\Lambda_L = 60°$

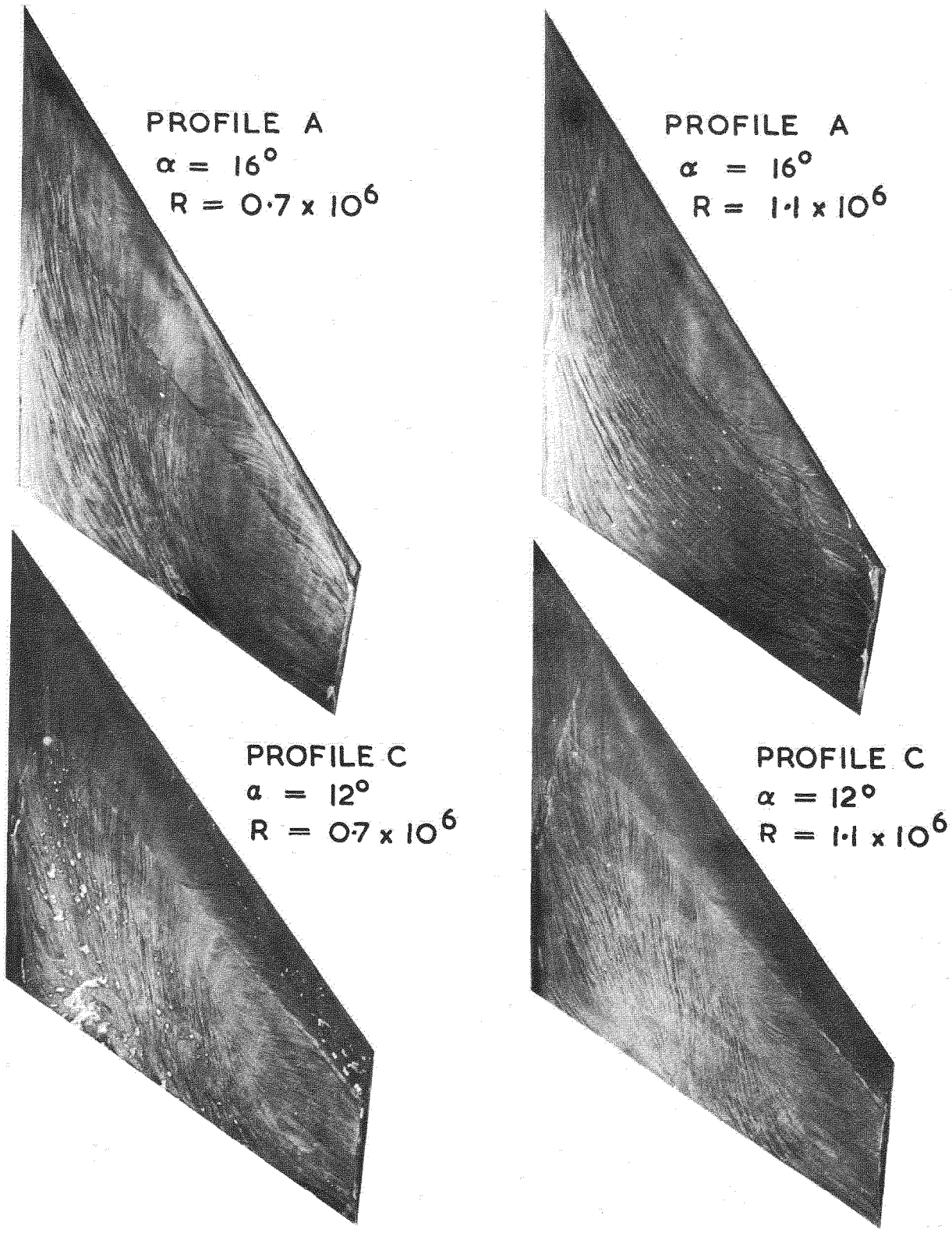

OIL PATTERNS SHOWING EFFECT OF REYNOLDS NUMBER

As the Photostat process is uneconomic owing to the large number of copies required for the Current Papers Series, Figs. 3a to 6 are half-tone lithographic reproductions from illustrations prepared by the improved procedure.

NPL/AERO/415

FIG. 7

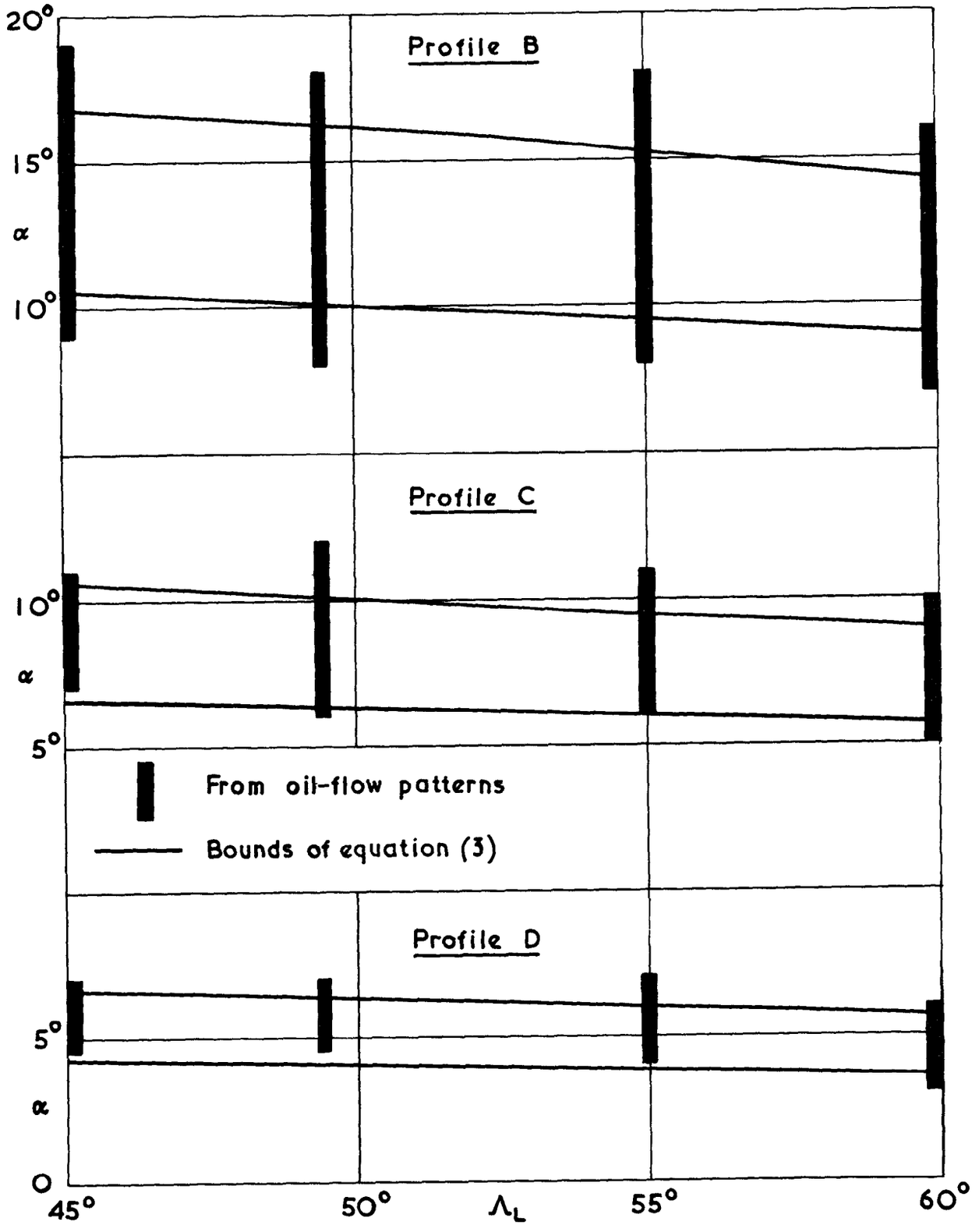

Ranges of incidence for part-span vortex layers

NPL/AERO/415

FIG. 8

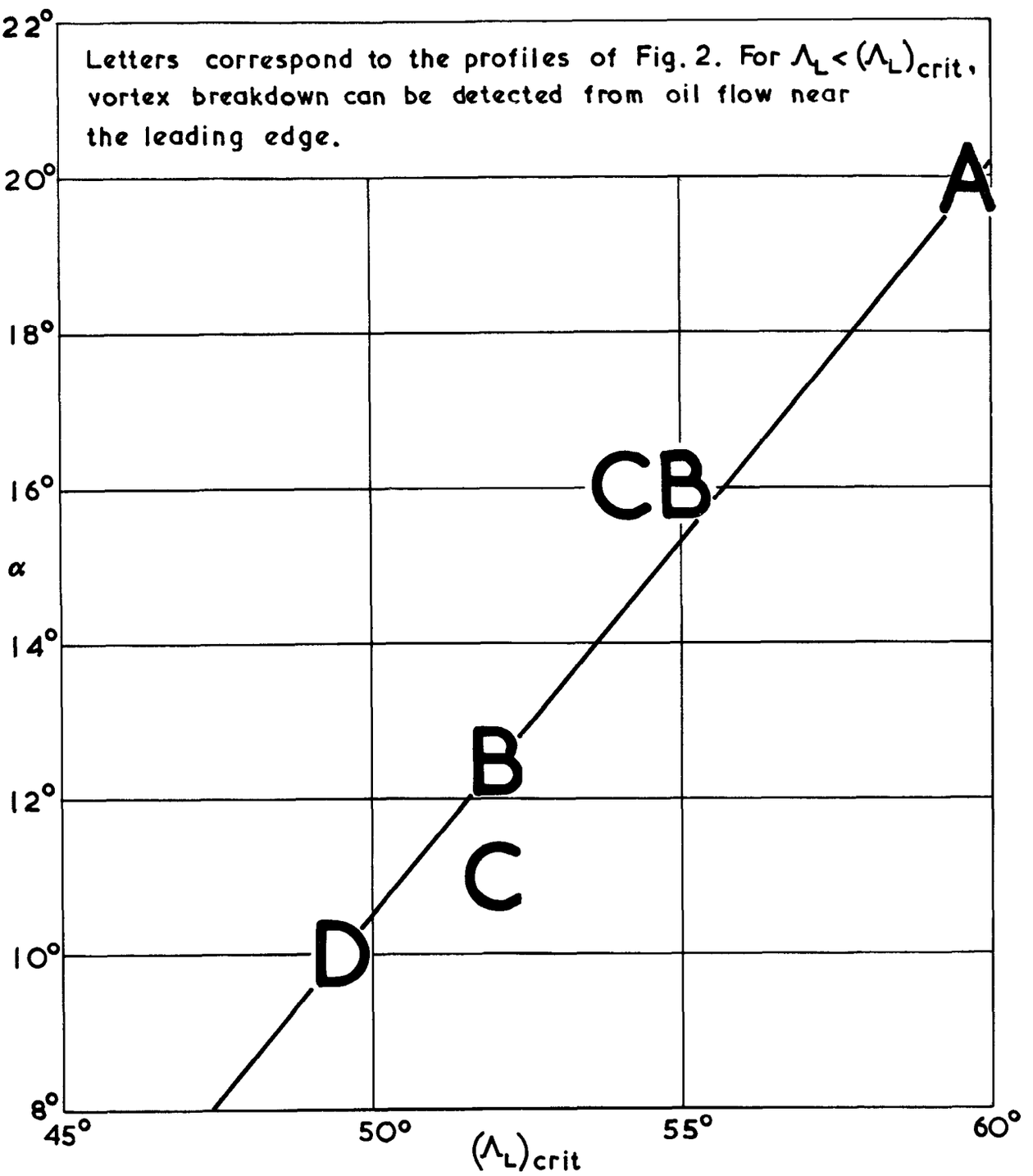

Critical leading-edge sweepback for vortex breakdown

DS 67718/1/Wt.61 K4 9/62 XL & CL

A.R.C. C.P.583
March, 1961
Garner, H. C. and Cox, Miss D. K. - Aero. Div., N.P.L.

SURFACE OIL-FLOW PATTERNS ON WINGS OF DIFFERENT LEADING-EDGE RADIUS AND SWEEPBACK

Oil-flow patterns have been studied on a series of models having four different angles of sweepback and four profiles of different nose radius. The patterns show that the phenomenon of leading-edge flow reversal is hardly influenced by nose radius. Numerical analysis leads to a rough formula for the range of incidence during which the origin of the leading-edge vortex traverses the leading edge from tip to root.

A.R.C. C.P.583
March, 1961
Garner, H. C. and Cox, Miss D. K. - Aero. Div., N.P.L.

SURFACE OIL-FLOW PATTERNS ON WINGS OF DIFFERENT LEADING-EDGE RADIUS AND SWEEPBACK

Oil-flow patterns have been studied on a series of models having four different angles of sweepback and four profiles of different nose radius. The patterns show that the phenomenon of leading-edge flow reversal is hardly influenced by nose radius. Numerical analysis leads to a rough formula for the range of incidence during which the origin of the leading-edge vortex traverses the leading edge from tip to root.

A.R.C. C.P.583
March, 1961
Garner, H. C. and Cox, Miss D. K. - Aero. Div., N.P.L.

SURFACE OIL-FLOW PATTERNS ON WINGS OF DIFFERENT LEADING-EDGE RADIUS AND SWEEPBACK

Oil-flow patterns have been studied on a series of models having four different angles of sweepback and four profiles of different nose radius. The patterns show that the phenomenon of leading-edge flow reversal is hardly influenced by nose radius. Numerical analysis leads to a rough formula for the range of incidence during which the origin of the leading-edge vortex traverses the leading edge from tip to root.

Printed and published by
HER MAJESTY'S STATIONERY OFFICE

To be purchased from
York House, Kingsway, London, W.C.2
423 Oxford Street, London W.1
13A Castle Street, Edinburgh 2
109 St. Mary Street, Cardiff
39 King Street, Manchester 2
50 Fairfax Street, Bristol 1
35 Smallbrook, Ringway, Birmingham 5
80 Chichester Street, Belfast 1
or through any bookseller

Printed in England

S.O. Code No. 23-9012-83